DOE/BC/15301-1
(OSTI ID: 808749)

Seismic Determination of Reservoir Heterogeneity: Application to the Characterization of Heavy Oil Reservoirs

Annual Report

Report Period: 09/01/2000 - 08/31/2001

Matthias G. Imhof

June 2002

DE-FC26-00BC15301

Matthias G. Imhof

Department of Geological Sciences

Virgina Tech

4044 Derring Hall (0420)

Blacksburg, VA 24061

James W. Castle

Department of Geological Sciences

Clemson University

340 Brackett Hall

Clemson, SC 29634-0976

Disclaimer

Abstract

The objective of the project is to examine how seismic and geologic data can be used to improve characterization of small-scale heterogeneity and their parameterization in reservoir models. We performed a theoretical and numerical study to examine which subsurface features the surface-seismic method actually resolves. For the Coalinga seismic dataset, we found that the deterministic resolution limit to be at 5 m. Thinner features need to be resolved statistically.

Hence we derived an algorithm which estimates seismic heterogeneity from fully processed seismic data volumes. With a preliminary 2-D implementation, we observed that seismic heterogeneity varies strongly with position in the seismic data volume. Most stochastic reservoir models are based on the assumption of regionally invariant statistics. Our findings motivate us to develop a new stochastic reservoir simulator which takes advantage of the increased resolution and spatial variations of the statistical reservoir parameters.

Contents

List of Figures

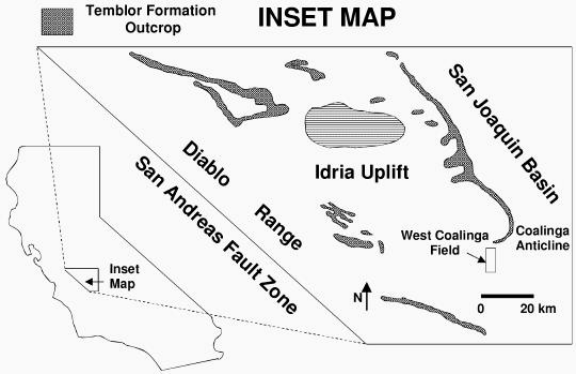

Figure 1: Location map of the Coalinga area, California.

1 Introduction

The objective of the project is to examine how seismic data can be used to parameterize models of small-scale reservoir heterogeneity. Although these heterogeneities cannot be resolved individually (deterministically) using seismic data, one can at least attempt to estimate their statistical properties from seismic data.

Reservoir characterization is an essential step in delineation, development, and production of hydrocarbon reserves. Our test area, the giant Coalinga field in California's San Joaquin Valley, is a good example. Large-scale steam-flood projects have been utilized for many years in order to enhance recovery of heavier oil. Steam-floods are costly to operate due to the necessary infrastructure and their energy consumption. Optimally, injected steam would spread evenly from the injection point and push the oil toward the producer wells. In reality, the steam patterns are very complex. Reservoir characterization provides an improved understanding of the reservoir and the movement of steam, which will help to increase the profitability by reducing steam injection which decreases the environmental impact of steam injection. Reservoir heterogeneity affects not only the steam flood, but also the production. The Coalinga reservoirs are strongly compartmentalized which is aggravated by the high oil viscosity. Reservoir characterization helps siting infill wells to produce bypassed oil to increase ultimate recovery.

Knowing the details of the reservoir allows simulation of different injection or production sce-

narios. The problem, however, is to build an accurate and suitable reservoir model that includes small-scale heterogeneity. Locally, boreholes yield an excellent description of the vertical heterogeneity at different spatial scales ranging from centimeters to hundreds of meters. Most of the time, the lateral heterogeneity cannot be derived from well data because of the large distances between wells. The most abundant data are seismic data, but their resolution is only on the order of tens of meters which is typically insufficient to resolve geological heterogeneities. Features smaller than a seismic quarter wavelength cannot be resolved with certainty. Yet the geology exhibits many small-scale features which may have a pronounced effect on the reservoir. For example, a clay drape is invisible on the seismic data but poses an impenetrable barrier to steam and oil. By combining seismic and well data, a deterministic framework is traditionally constructed which contains the major stratigraphic features. Small-scale features are filled in using statistical methods conditioned to well data and outcrops. The parameters for the fill-in process are often provided by measurements of analogous outcropping formations, analogous mature reservoirs with a dense well spacing, horizontal wells, pressure and production tests, or simply by accepting the default parameters of the modeling packet.

The objective of the project is to examine how seismic and geologic data can be used to describe small-scale heterogeneity and parameterize the reservoir models. Although these heterogeneities cannot be resolved individually (deterministically) using seismic data, we attempt to estimate their statistics from seismic data. The Coalinga field contains more than 2000 wells which provide the unusual luxury that even small-scale heterogeneity can be characterized with well data. The site allows construction of reservoir models from either seismic data or wireline logs and outcrops. Since these data are independent, the models can be compared and validated against each other. Ultimately, integration of seismic and geologic data and models will lead to a new level of understanding of the complex Coalinga field (Clark et al., 2001).

2 Executive Summary

The objective of the project is to examine how seismic data can be used to improve characterization of small-scale heterogeneity and their parameterization in reservoir models. As a first step, we performed a theoretical and numerical study to examine which features of a velocity-depth profile the surface-seismic method actually resolves. In a second step, we derived and implemented an algorithm which estimates seismic heterogeneity from fully processed and migrated 2-D or 3-D seismic data volumes.

We found that in a complex medium without sharp transitions, the reflection method is most sensitive to features at spatial scales similar to one quarter of the propagating wavelength. These features tune or interfere constructively with the seismic wavelength and, therefore, provide the strongest amplitude reflections. Thinner features have increasingly weaker amplitudes. Features thinner than one eighth of the wavelength are below deterministic resolution with surface-seismic methods. Instead, the statistical properties of a stack of thin features may be contained in the seismic data. The seismic wave passes through each of these thin features without reflection, but a stack of thin features composes a thick feature which may again be resolved deterministically. Features thicker than half a wavelength do not cause reflections either. Thick features simply perturb the traveltimes of deeper reflections. In the study area, the one-eighth wavelength resolution limit is around 5 m. For the Coalinga study site, we expect that features with thicknesses below 5 m can only be resolved statistically.

Hence, we developed seismic attributes which estimate heterogeneity contained in 2-D or 3-D seismic data volumes. The proposed seismic attributes measure the average medium heterogeneity from a 3-D seismic datacube. The basic idea behind the heterogeneity cube is that small-scale heterogeneity causes a small-scale footprint on seismic data, whose statistics relate to the statistics of the heterogeneity. Fitting the footprint statistics with model statistics, one obtains a set of seismic attributes which are interpretable as acquisition and processing footprints, stratigraphic or lithologic heterogeneity, or structural heterogeneity. Clearly, seismic heterogeneity could just be an artifact of the data acquisition or processing. These artifacts, however, can be removed by data processing. The seismic heterogeneity could relate to structural features such as sets of joints or fractures. The heterogeneity parameters would then relate to spacing, orientation, and density of fractures or joints. The last interpretation is lithologic or stratigraphic. If a layer is a composite of smaller sedimentary bodies, then each layer may exhibit numerous short-scale variations of the material properties. The seismic heterogeneity parameters may denote average dimensions and orientations of such small sedimentary bodies.

We developed a preliminary algorithm which operates on 2-D slices of fully processed and migrated seismic data. Pseudo-3-D results can be estimated by combining the results from two intersecting slices of data. The two results, however, may not be compatible. In the future, the algorithm will be expanded to operate with 3-D data volumes which ensures consistency of the results. With the preliminary algorithm, we observed that seismic heterogeneity varies strongly with position in the seismic data volume. Most methods to build stochastic reservoir models, however, assume that the statistics are at least regionally invariant. As a consequence, we will have to develop new modeling algorithms to take advantage of the increased resolution for the statistical reservoir parameters.

3 Results and Discussions

The West Coalinga field covers 18 square miles. ChevronTexaco Production Company in Bakersfield provided us with sample well logs as well as pre- and post-stack seismic data for the entire field. In conjunction with ChevronTexaco, the teams at Virginia Tech and Clemson University decided to focus on specific portions of sections 24D, 25D, and 36D. For a number of years, the Clemson team worked on other parts of the field. They shared geological information, core descriptions, additional wireline logs (originally from Chevron), and depositional environment interpretations with the Virginia Tech team to start the project.

The research during the first year was focused on two areas: (1) a numerical/theoretical study to determine which reservoir features cause seismic reflections, and hence, can be resolved on surface-seismic data; and (2) a preliminary algorithm in two dimensions to estimate heterogeneity in seismic datasets. In addition, Clemson University described a total of 920 m of continuous core from four wells stored at Chevron's warehouse in Richmond, California. The core from well 132A (IR85310), which is located just outside the study area in section 36D, was the most complete one. Wells 258A (IO06270) and 5-7T1 (IN50250) are located in the study areas of sections 36D and 25D, respectively. Well 4-15 (IO95320) is located in section 24D. ChevronTexaco Production Company in Bakersfield, CA, supplied the geophysical log data for wells within the study areas and granted access to the four cores used in this study. Lithofacies and bounding surfaces were identified in the cores studied. Depositional environments were interpreted based on detailed sedimentological description of the cores. Fourteen individual lithofacies were recognized, and four bounding surfaces were identified. The depositional environments are grouped into three facies tracts: estuarine, tide- to wave-dominated shoreline, and subtidal. Based on the study of surface outcrops and additional cores from West Coalinga field, these facies tracts, along with two others in the northern part of the field, can be correlated using cores and geophysical logs (Bridges and Castle, 2001).

3.1 Scale Dependence of Reflection Coefficients

Seismic velocities obtained from well logs commonly exhibit strong fluctuations over a range of depth scales. The exact nature of these fluctuations and the question of how to describe them have received much attention (e.g., Todoeschuck et al., 1992; Herrmann, 1997). The sampling interval of well logs is typically well below one meter. Seismic properties, on the other hand, estimated from surface seismic data can only be resolved on the scale of tens of meters. A common task is to link the two data sets with very different resolution levels (e.g., Poggiagliolmi and Allred, 1994; Ziolkowski et al., 1998) raising the question of which features resolved on well logs are detectable on seismic data. Widess (1973) declared that a layer embedded in a homogeneous medium is at the seismic resolution limit if its thickness is less than an eighth or, in the presence of noise, one fourth of the dominant wavelength. In a complex reservoir, however, layers might not be blocky, and one may ask what constitutes a detectable layer?

We addressed the question of scale dependency of seismic responses by calculating the reflection and transmission coefficients as functions of spatial scale contents of the medium. The spatial scale content of the model can be controlled by filtering in the wavelet domain which allows removal of localized features at a given scale. This technique of scale-filtering may also be useful for correlating wireline data against surface seismic data by removing details outside the scale bandwidth of the seismic data from log data.

The heterogeneity model for this study is based on an actual acoustic sonic log to avoid the problem of finding a stochastic or geological process to generate realistic heterogeneities. The sonic tool smoothes and samples the velocity profile (Hsu and Burridge, 1991) which provides the lower bound on the scale of measured heterogeneity. The length of the borehole yields the upper bound of spatial scale of heterogeneity. However, as a consequence of this approach, the results will be based on one, possibly not representative, well log.

3.1.1 Methodology

An actual acoustic sonic log is used to obtain a realistic heterogeneous velocity profile $v(z)$ as a function of depth z. To examine the scale dependence of reflection coefficients, the profile $v(z)$ is filtered by scale in the wavelet domain which allows removal of features of certain scales. The modified profile is then used as input to an acoustic layerstack method (e.g., Müller, 1985) to calculate reflection and transmission coefficients, frequency-dependent arrival times, and seismograms.

The velocity profile $v(z)$ is decomposed using a discrete wavelet transformation. The velocity profile input is filtered with a high-pass operator $\mathbf{H}$ whose coefficients, h_i, are determined by a discrete wavelet. For this study, the eight-coefficient symmetric Daubechies wavelet (1992), also known as fourth-order symlet, is used. The resulting profile contains the details under the first level of wavelet decomposition with the fourth-order symlet. The same velocity profile is also filtered with the orthogonal low-pass operator $\mathbf{L}$ which results in the first level approximation of the wavelet decomposition of the original velocity profile. The original profile can be reconstructed by recombining approximations and details using a set of dual operators $\mathbf{H}^*$ and $\mathbf{L}^*$.

The filters $\mathbf{L}$ and $\mathbf{H}$ are recursively applied until no further removal of details is possible. Schematically, the recursive decomposition, filtering of scales, and recursive reconstruction are shown in the following form.

$$v(z) = \mathbf{a}_0 \xrightarrow{\mathbf{L}} \mathbf{a}_1 \xrightarrow{\mathbf{L}} \mathbf{a}_2 \quad \cdots \quad \mathbf{a}_{J-1} \xrightarrow{\mathbf{L}} \mathbf{a}_J$$
$$\mathbf{a}_0 \xrightarrow{\mathbf{H}} \mathbf{d}_1 \qquad \mathbf{a}_1 \xrightarrow{\mathbf{H}} \mathbf{d}_2 \qquad \mathbf{a}_{J-1} \xrightarrow{\mathbf{H}} \mathbf{d}_J \tag{1a}$$

The vectors $\mathbf{a}_0$ to $\mathbf{a}_J$ are increasingly coarser approximations of the original velocity profile. The vectors $\mathbf{d}_0$ to $\mathbf{d}_J$ are increasingly longer details of the profile. Details at spatial scale level j are removed by setting the detail vector $\mathbf{d}_j$ at scale j to zero and recombining the remaining details

with the approximations.

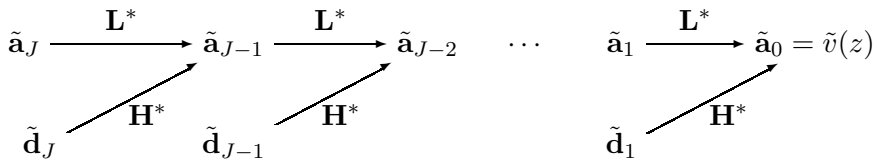

(1b)

Each level of details can be associated with a pseudo wavelength. It is defined as the wavelength ℓ_j of the spatial harmonic oscillation $\sin 2\pi z/\ell_j$ which locally best approximates the wavelet at detail level j. For the fourth-order symlet, the pseudo wavelength ℓ_j is given by (Matlab 6, 2001):

$$\ell_j = 1.4 \cdot 2^j \cdot \Delta\,, \tag{2}$$

where Δ is the sample spacing of the velocity profile. For a blocky layer, the pseudo thickness would be similar to twice the thickness of the layer.

We generated three different families of modified profiles: single-scale reconstructions, short-scale filtered, and long-scale filtered. In a single-scale reconstruction, all but details at one single level are removed. We will use the shorthand $\mathbf{a}_J$ & $\mathbf{d}_j$ to denote that the modified profile was reconstructed from the coarsest approximation at level J and details at level j. The recursive reconstruction becomes

$$\tilde{\mathbf{a}}_0 = \mathbf{H}^{*J} \cdot \tilde{\mathbf{a}}_J + \mathbf{H}^{*j-1} \cdot \mathbf{L}^* \cdot \tilde{\mathbf{d}}_j\,. \tag{3}$$

A family of profiles is generated by varying i from 1 to J.

For short-scale filtered profiles, the details at the shortest scales are omitted during the recursive reconstruction. The shorthand will be $\mathbf{a}_J$ & $\mathbf{d}_{j-J}$ to denote that the profile was constructed omitting scale levels smaller than j. The recursive reconstruction becomes

$$\tilde{\mathbf{a}}_0 = \mathbf{H}^{*J} \cdot \tilde{\mathbf{a}}_J \;+\; \mathbf{H}^{*j-1} \cdot \mathbf{L}^* \cdot \tilde{\mathbf{d}}_j \;+\; \ldots \;+\; \mathbf{H}^{*J-1} \cdot \mathbf{L}^* \cdot \tilde{\mathbf{d}}_J\,. \tag{4}$$

A family of progressively stronger filtered profiles is generated by letting j increase from 1 to J.

For long-scale filtered profiles, the details at the longest scales are omitted during the recursive

reconstruction. The shorthand will be $\mathbf{a}_J$ & $\mathbf{d}_{1-j}$ to denote that the reconstructed profile omits scale levels larger than j. The recursive reconstruction becomes

$$\tilde{\mathbf{a}}_0 = \mathbf{H}^{*J} \cdot \tilde{\mathbf{a}}_J \; + \; \mathbf{L}^* \cdot \tilde{\mathbf{d}}_1 \; + \; \mathbf{H}^* \cdot \mathbf{L}^* \cdot \tilde{\mathbf{d}}_2 \; + \; \ldots \; + \; \mathbf{H}^{*j-1} \cdot \mathbf{L}^* \cdot \tilde{\mathbf{d}}_j \, . \tag{5}$$

A family of progressively stronger filtered profiles is generated by letting j decrease from J to 1.

A modified velocity profile is interpreted as a stack of thin layers. This stack is embedded in a homogeneous fullspace whose velocity and density correspond to the average values of the layerstack. For every angular frequency ω, the complex valued seismic reflection and transmission coefficients $R(\omega)$ and $T(\omega)$ can be calculated using a layerstack scheme (e.g., Müller, 1985). The seismograms $R(t)$ and $T(t)$ are calculated by Fourier synthesis from $R(\omega)$ and $T(\omega)$ after weighting each with an appropriate source wavelet $S(\omega)$, e.g., the Ricker wavelet. Since the coefficients $R(\omega)$ and $T(\omega)$ account for the entire layerstack, primaries, multiples, direct wave, and the coda are all contained in the seismograms.

3.1.2 Example

For the velocity profile $v(z)$, a 624.23 m interval of an actual sonic log sampled at $\Delta z = 0.15\,\mathrm{m}$ ($= 0.5\,\mathrm{ft}$) was used. Altogether, there are $m = 4096$ samples which yield $J = 12$ levels of details. Figure 2 shows the original velocity profile and reconstructions from the coarsest approximation $\tilde{\mathbf{a}}_{12}$ with only one level of details. At the same depth, one may find details at different scales since stratigraphic units typically consist of smaller units of various thicknesses. An example is the high velocity formation between 575 and 650 m which dominates the details $\mathbf{d}_{10}$. This formation consists of two smaller units which are major features on the details $\mathbf{d}_8$. Moreover, any sharp transition is actually composed of details of numerous different scales. Figure 3 shows the velocity profiles filtered by short scales and long scales. For the short-scale filters, the shortest details and progressively longer ones are omitted in the reconstruction. In the case of long-scale filtering, the longest details and progressively shorter ones are omitted.

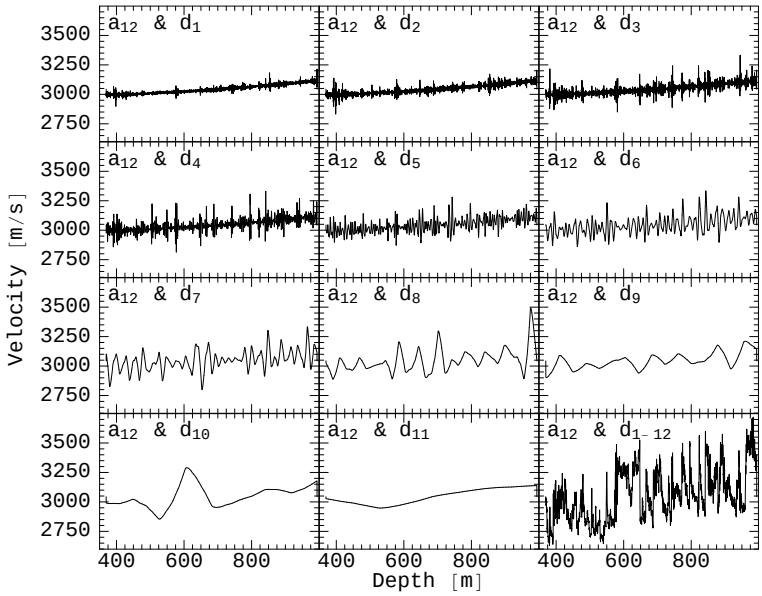

Figure 2: Wavelet filtered velocity profiles: only one level of details was used for reconstruction.

Reflection Seismograms: We present the reflection seismograms for two Ricker wavelets of 50 and 1000 Hz center frequency. The seismograms were calculated by convolving the Ricker wavelets with the Fourier transformation of $R(\omega)$ computed with the layerstack scheme.

Single-scale reconstruction.– Only the coarsest approximation $\mathbf{a}_{12}$ and one level of detail $\mathbf{d}_j$ were used to construct the velocity profiles. The corresponding synthetic reflection seismograms are shown in Figure 4. At 50 Hz, the reflections are predominantly caused by the details $\mathbf{d}_6$, $\mathbf{d}_7$, and $\mathbf{d}_8$; while at 1 kHz, mainly the details $\mathbf{d}_2$, $\mathbf{d}_3$, and $\mathbf{d}_4$ appear to have an effect. The seismograms at 1000 Hz are affected the most by the details $\mathbf{d}_3$, while seismograms at 50 Hz are affected the most by $\mathbf{d}_7$. Not only are the resulting amplitudes the largest, but even the waveforms are remarkably similar to the ones for the complete velocity profile, although some of the events appear to arrive with slight shifts of time. The details $\mathbf{d}_7$ and $\mathbf{d}_3$ have pseudo wavelengths $\ell_7 = 27.3$ m and $\ell_3 = 1.7$ m, which are similar to half the average wavelengths of 60.8 and 3.0 m of the propagating Ricker wavelets at 50 and 1000 Hz.

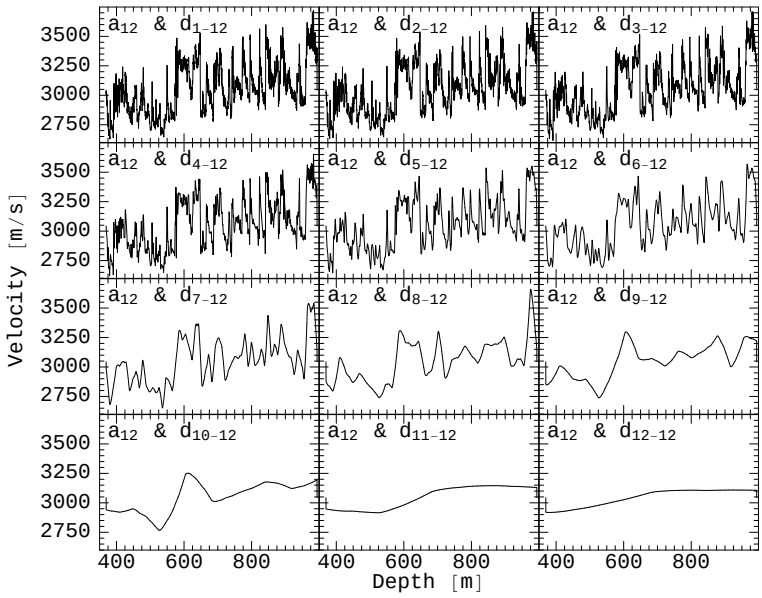

(a)

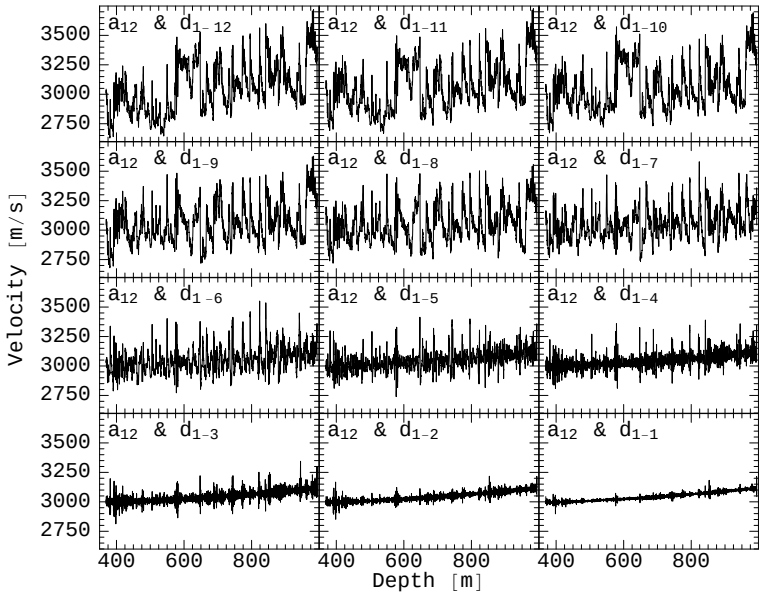

(b)

Figure 3: Wavelet filtered velocity profiles with ranges of details removed: (a) short-scale filtered where the shortest scale and progressively longer ones are removed, (b) long-scale filtered where the longest scale and progressively shorter ones are omitted.

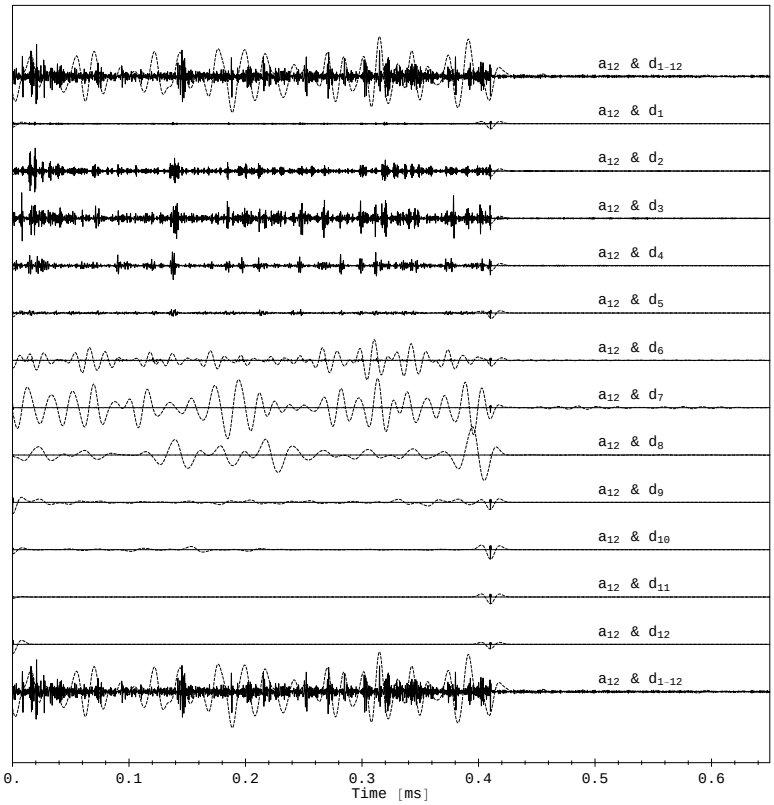

Figure 4: Reflection seismograms for single-scale reconstructions with only one level of details. The center frequencies of the propagating Ricker pulses are 1 kHz (solid) and 50 Hz (dashed). The first and last events are caused by the discontinuities between the homogeneous fullspace and the embedded layerstack.

Short-scale filtering.– Figure 5(a) shows that removing the details of the shortest scale, and then consecutively longer ones, hardly changes reflection waveforms until details on the order of half the dominant wavelength are eliminated. Beyond this threshold scale, major reflections and coda-like events vanish rapidly with levels.

Long-scale filtering.– Figure 5(b) shows that removal of the longest scale and successive omission of shorter ones leads to subtle shifts in arrival times while preserving amplitudes and waveforms. Below the threshold of half the dominant wavelength, waveforms are strongly affected by progressive filtering of scales as seismic amplitudes vanish rapidly with levels.

The removal of either shortest or longest details appears to perturb the resulting reflection

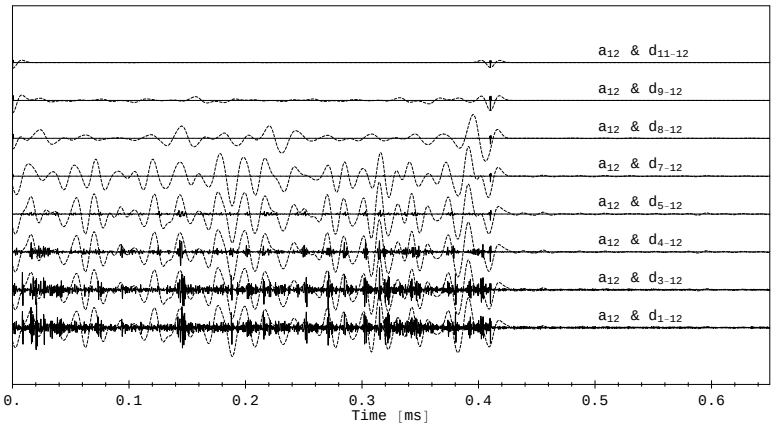

(a)

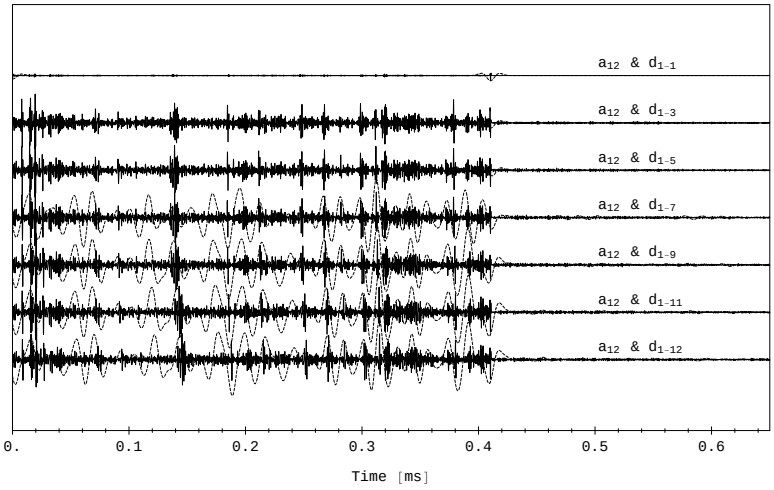

(b)

Figure 5: Reflection seismograms as a function of model scale content for (a) short-scale filtered profiles, and (b) long-scale filtered ones. The center frequencies of the propagating Ricker pulses are 1 kHz (solid) and 50 Hz (dashed).

seismograms only slightly which suggests that the reflection seismogram is controlled by spatial scales similar to half the dominant wavelength. This inference is consistent with the findings in diffraction tomography. Wu and Toksöz (1987) found that assuming single scattering, a wave propagating in the vertical direction with a wavenumber k (wavelength λ) is scattered back in the vertical direction predominantly by slowness heterogeneities of wavenumber $2k$ (or wavelength

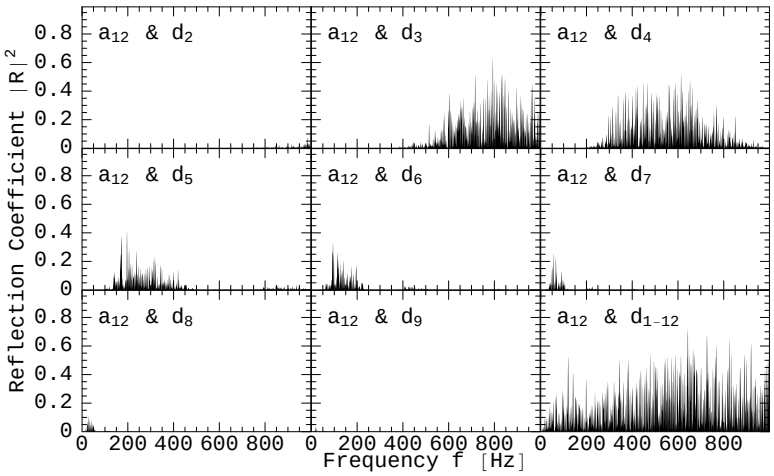

Figure 6: Magnitudes of reflections as functions of model scale content and propagating frequency for single-scale model reconstructions.

$\lambda/2$).

Reflection Coefficients: The reflection coefficients $\left|R(\omega)\right|^2$ are presented in Figures 6 and 7.

Single-scale reconstructions.– Figure 6 presents the reflection coefficients as functions of frequency and the level of detail used for the reconstruction of the velocity profiles. For every level of detail, there is a frequency band where significant reflection occurs. For the example of the reconstruction $\mathbf{a}$ & $\mathbf{d}_7$, the reflective frequency band is $25-100\,\mathrm{Hz}$ with maximal reflection around $50\,\mathrm{Hz}$. At $50\,\mathrm{Hz}$, the average wavelength $60.8\,\mathrm{m}$ is approximately twice the pseudo wavelength $\ell_7 = 27.3\,\mathrm{m}$. Similar observations are made for every level of detail: details with a given pseudo wavelength ℓ reflect the band of propagating wavelengths λ from $\ell \leq \lambda \leq 4\ell$ with a maximum at 2ℓ. An interesting observation is the presence of secondary reflective bands located around propagating wavelengths $\lambda/2$ and $\lambda/4$.

Short-scale filtering.– Figure 7(a) illustrates the reflection coefficients as functions of frequency for short-scale filtered velocity profiles where details of the shortest scale and consecutively longer ones are eliminated. For every reconstruction $\mathbf{a}_{12}$ & $\mathbf{d}_{j-12}$, there is a cut-off frequency at which

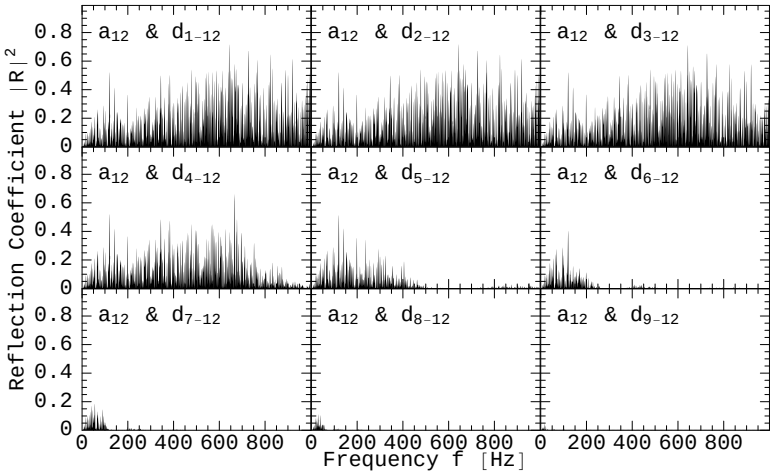

(a)

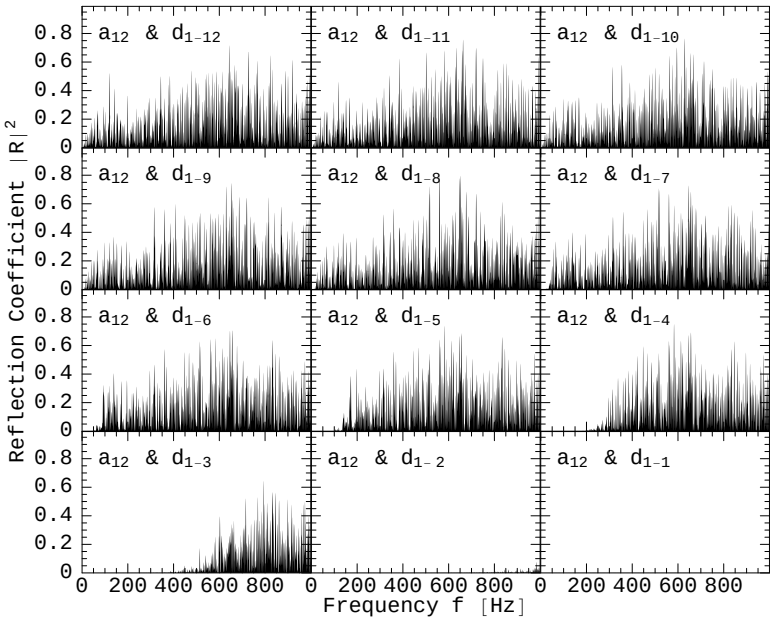

(b)

Figure 7: Magnitudes of reflections as functions of model scale content and propagating frequency: (a) for short-scale filtered, and (b) for long-scale filtered velocity profiles.

reflections vanish. Below this cut-off frequency, the reflection coefficients are not perturbed by the removal of short-scale details in the velocity profile. The reconstructed profile $\mathbf{a}_{12}$ & $\mathbf{d}_{5-12}$, for example, only reflects frequencies up to 500 Hz. For this profile, the shortest pseudo wavelength

$\ell_5 = 6.7\,\mathrm{m}$ is comparable to the average wavelength of 6.0 m at 500 Hz. Similar observations can be made for every short-scale filtered profile. If the shortest pseudo wavelength in the profile is ℓ, then propagating wavelengths $\lambda < \ell$ are not reflected in a significant manner. Again, secondary reflective-wavelength bands are observed around $\lambda/2$ and $\lambda/4$.

Long-scale filtering.– In contrast to the results of short-scale filtering, the effect of removing the longest scale and then progressively shorter ones is quite different as demonstrated in Figure 7(b). For every velocity profile, there is a cut-off frequency below which no significant reflections occur. At frequencies above the cut-off, the reflection coefficients are perturbed by the long-scale filtering, although some reflection peaks can be correlated between panels of reflection coefficients for different detail contents. If the longest pseudo wavelength in the velocity profile is ℓ, then wavelengths $\lambda > 4\ell$ are not reflected significantly.

The interpretation from Figures 6 and 7 is that the low-frequency reflectivity is not affected by details with short pseudo wavelengths. From numerical studies, Folstad and Schoenberg (1992) concluded that fine layering of the order 1/10 of the wavelength or less can be replaced by thicker and possibly anisotropic layers. Removing short-scale heterogeneities does not change the overall reflection spectrum. The reflection coefficients at low frequencies vanish once the wavelength λ is more than four times larger than the pseudo wavelength ℓ. Removing long scales, however, affects wave propagation at all frequencies. In the discussion, I will argue that the primary and secondary reflection bands are caused by constructive interference of reflections, but the amplitudes of the secondary reflection bands are greatly reduced because the details are smooth with long pseudo wavelengths ℓ compared to the propagating wavelength λ.

3.1.3 Discussion and Conclusions

The objective of this study was to determine how different spatial scales affect reflection. The sonic log was converted to slowness, scale-filtered in the wavelet domain, and transformed back to obtain scale-filtered velocity profiles. The resulting profiles have some of their details at short and/or long scales removed. These modified profiles were used to calculate reflection from a layerstack as

functions of time, frequency, and scale content of the profiles. All findings are based on only one, possibly not representative, well log.

Single-scale reconstructions, i.e., modified profiles containing one scale of details and the coarsest approximation, demonstrated that only a few scales contributed to reflection events. A propagating wavelength λ is predominantly affected by details of pseudo wavelengths $\ell \leq \lambda \leq 4\ell$ with maximum effect at $\lambda = 2\ell$. A classical homogeneous layer of thickness $\lambda/4$ is best represented by a symlet with pseudo wavelength $\ell = \lambda/2$, since the layer roughly corresponds to the main positive peak of the wavelet. Such a layer, however, will exhibit the maximal reflection amplitude since reflections from the top and the bottom interfere constructively, an effect often referred to as tuning. Hence, one might speculate that details with pseudo wavelength $\ell = \lambda/2$ are the most reflective because they tune the dominant, propagating wavelength λ. Based on wavelet interference studies, Widess (1973) declared a thin layer of thickness $\lambda/8$ to be at the theoretical threshold of resolution. A $\lambda/8$ layer, however, corresponds to a detail of pseudo wavelength $\ell = \lambda/4$ which was identified in this study as the shortest scale of practical importance. The longest scale of importance is $\ell = \lambda$ which corresponds to a layer of thickness $\lambda/2$, exactly the thickness at which Widess (1973) observed the onset of constructive wavelet interference. For any thicker layer, one would observe two distinct reflection events. Hence, one might postulate that the pseudo wavelengths $\ell \leq \lambda \leq 4\ell$ dominate the reflection of wavelength λ because they all enhance the amplitudes through constructive interference, i.e., tuning. For any pseudo wavelength, the higher-order reflection bands observed on Figure 6 occur again at wavelengths which would interfere constructively when interacting with features of that scale.

From short-scale filtering, i.e., the removal of the shortest and progressively longer details, we found that scales with pseudo wavelengths ℓ less than one-fourth the propagating wavelength λ hardly affect reflection. In our models, this next shorter scale was of dimension $\ell = \lambda/8$. This finding is not inconsistent with the conclusion by Folstad and Schoenberg (1992) that fine layering on the order of $1/10\lambda$ or less does not affect seismic wave propagation other than rendering the medium anisotropic. Equivalent medium theory based on Backus (1962) averaging can be applied

to replace the thin layers by thicker but anisotropic ones.

From long-scale filtering, i.e., the removal of the longest details and progressively shorter ones, we observed that details with pseudo wavelength ℓ larger than the propagating wavelengths λ have little effect on reflection with the exception of timeshifts between different events within the coda. The removal of long details may increase or decrease the local velocities, some coda events can be advanced while others are retarded.

Some findings of this study appear to contradict everyday experience. According to the presented results, a blocky layer model should not reflect at high frequencies. In practice, a boundary between two large stratigraphic units may also be the boundary between smaller subunits of scales compatible with reflection of short wavelengths. Furthermore, sharp discontinuities cannot be represented with a generic wavelet, e.g., the fourth-order symlet, at only one scale. Rather, details at numerous scales are needed to represent the discontinuities. Hence, even if a blocky layer is much thicker than the wavelength, the bounding discontinuities will require the presence of wavelets at scales comparable to the wavelength.

3.2 2-D Estimation of Seismic Heterogeneity

We developed a preliminary algorithm which measures the average heterogeneity in a window of seismic data. The heterogeneity is quantified by two characteristic correlation lengths and one orientation. Using a sliding window, these attributes are estimated for every point in a 2-D or 3-D seismic dataset. The resulting attribute volumes form the heterogeneity cubes which may aid the interpretation of seismic data and could provide novel information for reservoir characterization and model building. They could also be used to condition stochastic reservoir models.

For windows of seismic data, the proposed seismic attributes measure the average heterogeneity. The basic idea behind the heterogeneity cube is that small-scale heterogeneity causes a small-scale footprint on seismic data, whose statistics relate to the statistics of the heterogeneity. Parameterizing the footprint statistics, one obtains a set of seismic attributes which are interpretable as acquisition and processing footprints, stratigraphic or lithologic heterogeneity, or structural het-

erogeneity. Acquisition and processing footprints may be removable with algorithms described by Marfurt et al. (1998), Canning and Gardner (1998), or Soubaras (2002). From the stratigraphic viewpoint, the parameters may denote average dimensions and orientations of small sedimentary bodies (Imhof and Toksöz, 2000), while the parameters might relate to average size, spacing, and orientations of fractures and joints for the structural point of view. The heterogeneity cubes nicely complement the coherency cube (Bahorich and Farmer, 1995). The low-pass heterogeneity cube measures the average fluctuation of the seismic signal within a window, while the high-pass coherency cube detects subtle changes in the signal, e.g., when crossing faults or facies.

3.2.1 Method

In their current formulation, the heterogeneity attributes are window attributes, i.e., they are obtained from a window $w(x,z)$ centered at (x,z) of poststack data $d(i,j)$. The local crosscorrelation function ($LCCF$) $\hat{R}$ is estimated between the window w and the dataset d:

$$\rho(k,l) = \frac{1}{N} \sum_{i,j \in w} w(i,j) d(i+k, j+l) \tag{6}$$

and

$$\hat{R}(k,l) = \frac{\rho(k,l)}{\rho(0,0)}\,, \tag{7}$$

where N is the number of non-zero terms in the summation for correlation lags (k,l). Depending on the number of computed lags, however, $\hat{R}$ might be large with numerous coefficients. To obtain useful seismic attributes, the number of parameters is being reduced by fitting the data ACF $\hat{R}$ with a model ACF $\bar{R}$ containing only a small number of free parameters. Presently, an anisotropic Gaussian function is used for the model ACF $\bar{R}$ (Imhof and Toksöz, 2000),

$$\bar{R}(k,l;a,b,\phi) = \exp\left(-\frac{(k\cos\phi + l\sin\phi)^2}{a^2} - \frac{(l\cos\phi - k\sin\phi)^2}{b^2} \right)\,, \tag{8}$$

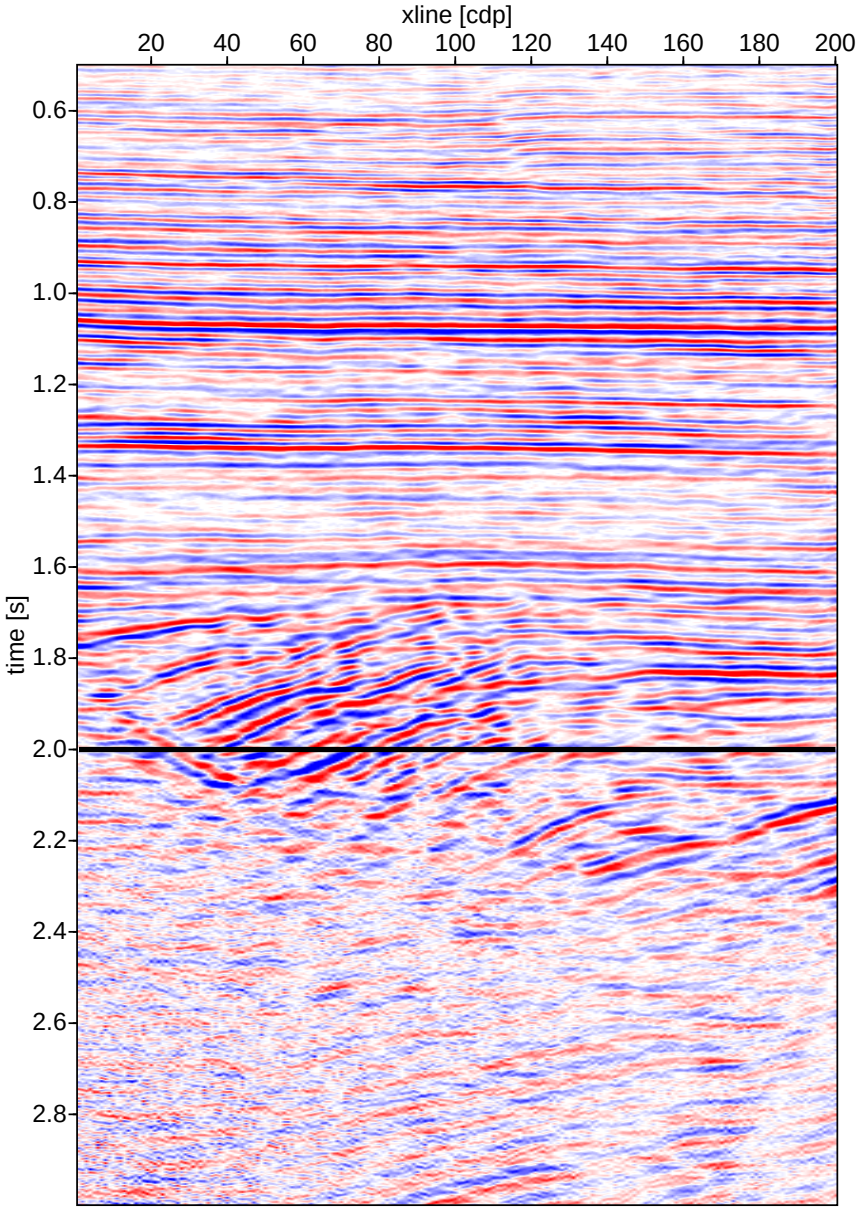

Figure 8: Seismic amplitudes for inline section 50. The flat Frio reflections overlay the severely faulted Vicksburg section. The heavy black line denotes the location of the timeslice.

although other forms, e.g., spherical or exponential, are possible, too (Lantuéjoul, 2002). The free parameters are: a long characteristic length a, a short characteristic length b, and the orientation ϕ of the length a. A proper subset of the parameter space is systematically scanned to determine the optimal triplet (a, b, ϕ) which minimizes the difference between the model ACF $\bar{R}(k, l)$ and the

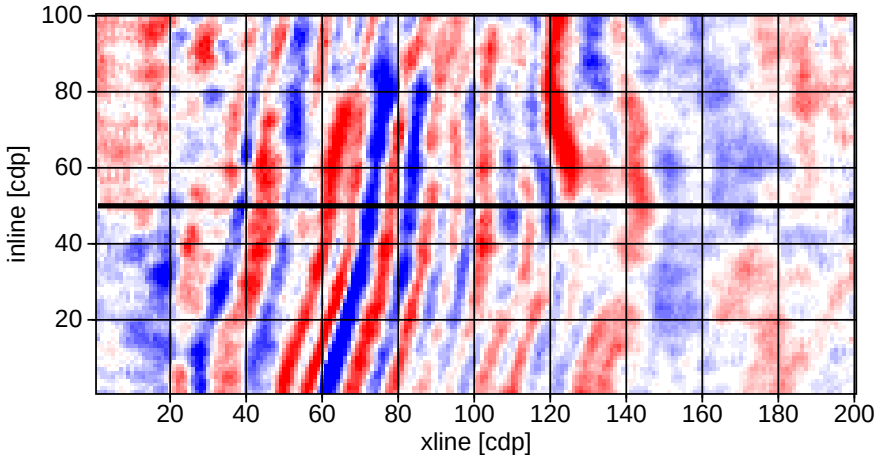

Figure 9: Seismic amplitudes for timeslice 2.0 s. The heavy black line denotes the location of the inline.

data ACF $\hat{R}(k,l)$.

$$\epsilon^2 = N^{-1} \sum_{k,l} \left(\hat{R}(k,l) - \bar{R}(k,l) \right)^2 \tag{9}$$

The parameters a, b, and ϕ, plus the misfit ϵ, constitute the heterogeneity attributes at location (x,z). By choosing different center points and repeating the procedure, one may compute two or three-dimensional images of the heterogeneity parameters which constitute the heterogeneity cubes.

Example: The heterogeneity attributes are calculated for one timeslice at 2000 ms of the 3-D poststack datacube from the Stratton field in south Texas (e.g., Hardage et al., 1994). The dataset is commonly used for testing of seismic interpretation methods because it has been put into the public domain which facilitates comparison, presentation, and publication. The window probe spans 19 by 19 traces. Figures 8 and 9 present inline section 50 and a timeslice at 2.0 s. The corresponding heterogeneity attributes are shown in Figures 10 to 13.

The amplitudes (Figure 8) reveal that the stratigraphy is basically flat layers overlaying the severely faulted Vicksburg section. These trends are detected by the attributes shown in Figures 10 to 13. Even in flat lying areas, however, all seismic heterogeneity attributes exhibit strong variations which may indicate that the spatial statistics of small-scale stratigraphic heterogeneity depend

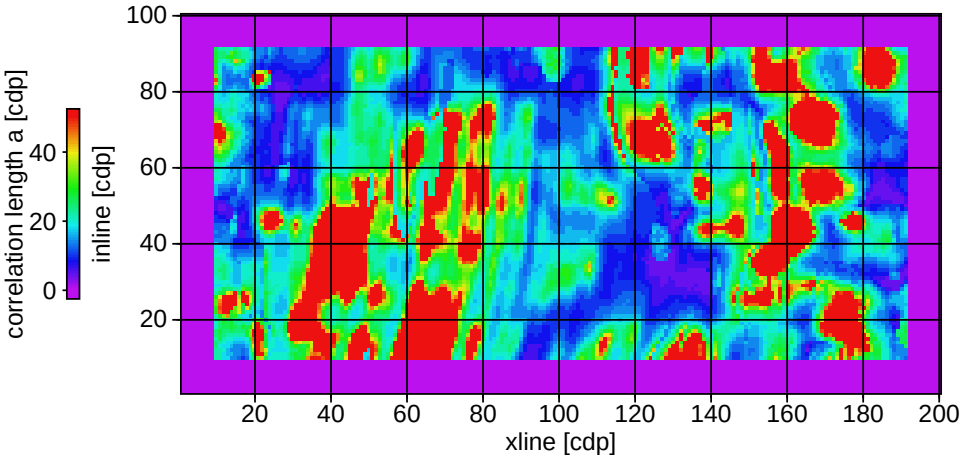

Figure 10: Heterogeneity parameters: long correlation length a for timeslice.

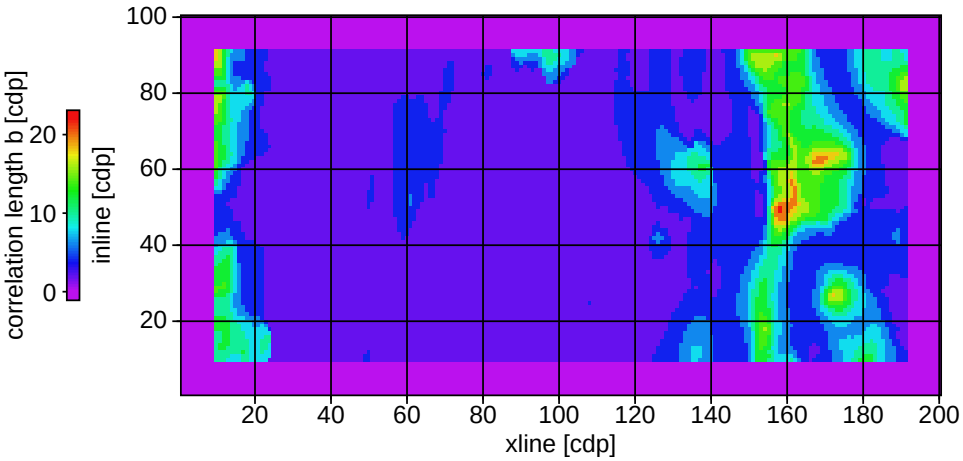

Figure 11: Heterogeneity parameters: short correlation length b for timeslice.

are instationary meaning that they are location dependent. This hypothesis requires more work. Extending the algorithm to 3-D may change these findings. If the hypothesis withstands rigorous testing, however, we will need to develop new methods for reservoir modeling since current practice is often based on the assumption of stationary statistics.

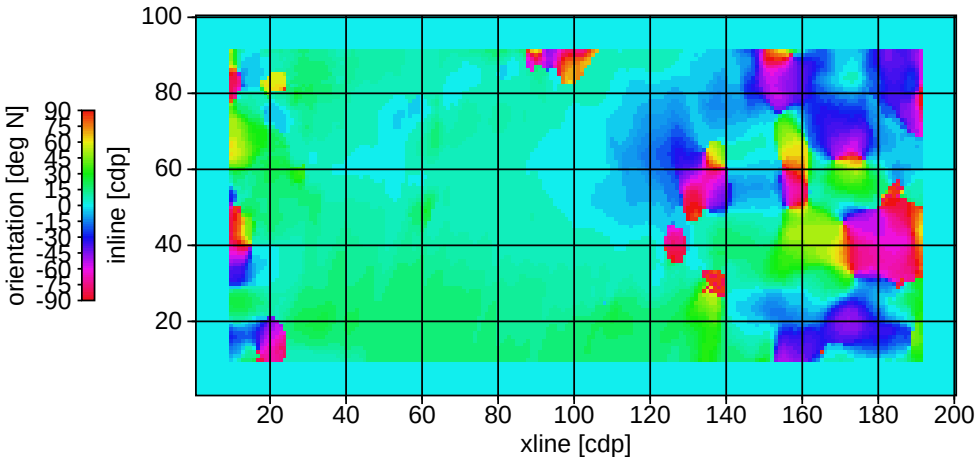

Figure 12: Heterogeneity parameters: orientation ϕ for timeslice.

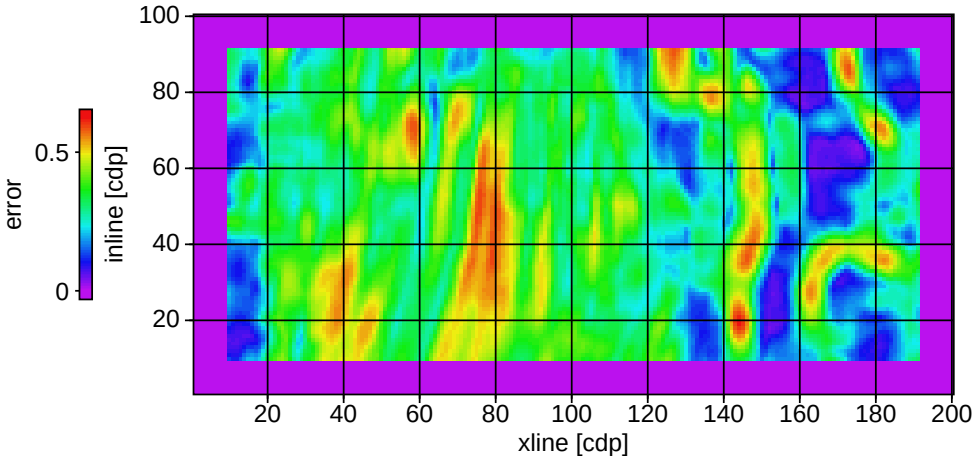

Figure 13: Heterogeneity parameters: misfit ϵ for timeslice.

4 Conclusions

In the first stage of the project, we performed a theoretical study to examine which subsurface features cause seismic reflections. We found that for our study area, the Coalinga oil field in California, the resolution limit is on the order of 5 m. Thinner features may not be resolvable anymore with surface-seismic data. A collection of thin stratigraphic features may form a larger feature which reflects seismic energy. The reflection from the combined feature may contain statistical information about the individual features.

This resolution study will form the groundwork for a deterministic analysis of the seismic data. We will load the 3-D seismic dataset provided by ChevronTexaco into a state-of-the-art seismic interpretation system to examine which stratigraphic motives we can detect, resolve, and characterize without resorting to statistical techniques. Modern systems nearly allow a sample-wise interpretation of seismic data volumes which provides a tremendous resolution when combined with stratigraphic intuition. We intend to push these methods to their limit to study which level of detail we can see in the seismic data, and hence, which level of detail can be put into a reservoir model deterministically instead of statistically.

The theoretical resolution study will allow comparison between reservoir models based on either seismic data or well log data. In the second year, Clemson University under the guidance of Dr. Castle will begin a detailed geological study of the focus areas in sections 24D, 25D, and 36D of West Coalinga Field to examine and model the Coalinga reservoir using wireline data, well cores, and outcrops. The resolution study will help bridging between reservoir models obtained by seismic and geologic analysis.

We developed a preliminary algorithm which estimates the statistics of reservoir features from seismic data below the deterministic resolution limit. We observed that these statistics vary throughout the reservoir. We will need to extend the algorithm from 2-D to 3-D to better understand these fluctuations. In a later phase, we will need to find an algorithm to compute reservoir models compatible with these statistics. Ultimately, it may even be possible to condition the instationary simulations to the well data. Again, the geologic models will provide control and later

be used for integration.

5 References

G. E. Backus. Long wave anisotropy produced by horizontal layering. *J. Geophys. Res.*, 67: 4427–4440, 1962.

M. S. Bahorich and S. L. Farmer. 3-D seismic coherency for faults and stratigraphic features. *The Leading Edge*, 14(10):1053–1058, 1995.

R. A. Bridges and J. W. Castle. Application of outcrop analogs to reservoir characterization of shallow-marine and coastal-plain reservoirs: An example from the San Joaquin Basin, California. In *AAPG Annual Meeting*, 2001.

A. Canning and G. H. F. Gardner. Reducing 3-D acquisition footprint for 3-D DMO and 3-D prestack migration. *Geophysics*, 63(4):1177–1183, 1998.

M. S. Clark, L. F. Klonsky, and K. E. Tucker. Geologic study and multiple 3-D surveys give clues to complex reservoir architecture of giant Coalinga oil field, San Joaquin Valley, California. *The Leading Edge*, 20(7):744–751, 2001.

I. Daubechies. *Ten Lectures on Wavelets*. Society for Industrial and Applied Mathematics, Philadelphia, PA, 1992.

P. G. Folstad and M. Schoenberg. Low frequency propagation through fine layering. In *62nd Ann. Internat. Mtg., Soc. Expl. Geophys., Expanded Abstracts*, pages 1278–1281, 1992.

B. A. Hardage, R. A. Levey, V. Pendleton, J. Simmons, and R. Edson. 3-D seismic case history evaluating fluvially deposited thin-bed reservoirs in a gas-producing property. *Geophysics*, 59(11): 1650–1665, 1994.

F. Herrmann. *A scaling medium representation, a discussion on well-logs, fractals and waves*. PhD thesis, Delft University of Technology, 1997.

K. Hsu and R. Burridge. Effects of averaging and sampling on the statistics of reflection coefficients. *Geophysics*, 56(1):50–58, 1991.

M. G. Imhof and M. N. Toksöz. Estimation of stratigraphic heterogeneity using seismic reflection data. *J. Seis. Expl.*, 9(1), 2000.

C. Lantuéjoul. *Geostatistical Simulation: Models and Algorithms*. Springer, Berlin, 2002.

K. J. Marfurt, R. M. Scheet, J. A. Sharp, and M. G. Harper. Suppression of the acquisition footprint for seismic sequence attribute mapping. *Geophysics*, 63(3):1024–1035, 1998.

Matlab 6. The MathWorks, Inc., Natick, MA, 2001. Release 12.

G. Müller. The reflectivity method: a tutorial. *J. Geophys.*, 58:153–174, 1985.

E. Poggiagliolmi and R. D. Allred. Detailed reservoir definition by integration of well and 3-D seismic data using space adaptive wavelet processing. *The Leading Edge*, 13(7):749–754, 1994.

R. Soubaras. Attenuation of acquisition footprint for non-orthogonal 3D geometries. In *64th Mtg. Eur. Assoc. Geosci. and Eng., Extended Abstracts*, 2002.

J. P. Todoeschuck, M. Pilkington, and M. E. Gregotski. If geology is fractal, what do we do next? (round table). *The Leading Edge*, 11(10):29–35, 1992.

M. B. Widess. How thin is a thin bed. *Geophysics*, 38(5):1176–1254, 1973.

R. S. Wu and N. M. Toksöz. Diffraction tomography and multisource holography applied to seismic imaging. *Geophysics*, 52(1):11–25, January 1987.

A. Ziolkowski, J. R. Underhill, and R. G. K. Johnston. Wavelets, well ties, and the search for subtle stratigraphic traps. *Geophysics*, 63(1):297–313, 1998.

6 Bibliography

M.G. Imhof, 'The Heterogeneity Cube: a Family of Seismic Attributes', to be presented at the 71st Annual Internat. Mtg., Soc. Expl. Geophys., Expanded Abstracts.

M.G. Imhof, 'Scale Dependence of Reflection and Transmission Coefficients', *Geophysics*, submitted.